Selected papers from 10th International Conference on Computational Fluid Dynamics in the Oil & Gas, Metallurgical and Process Industries

Progress in Applied CFD
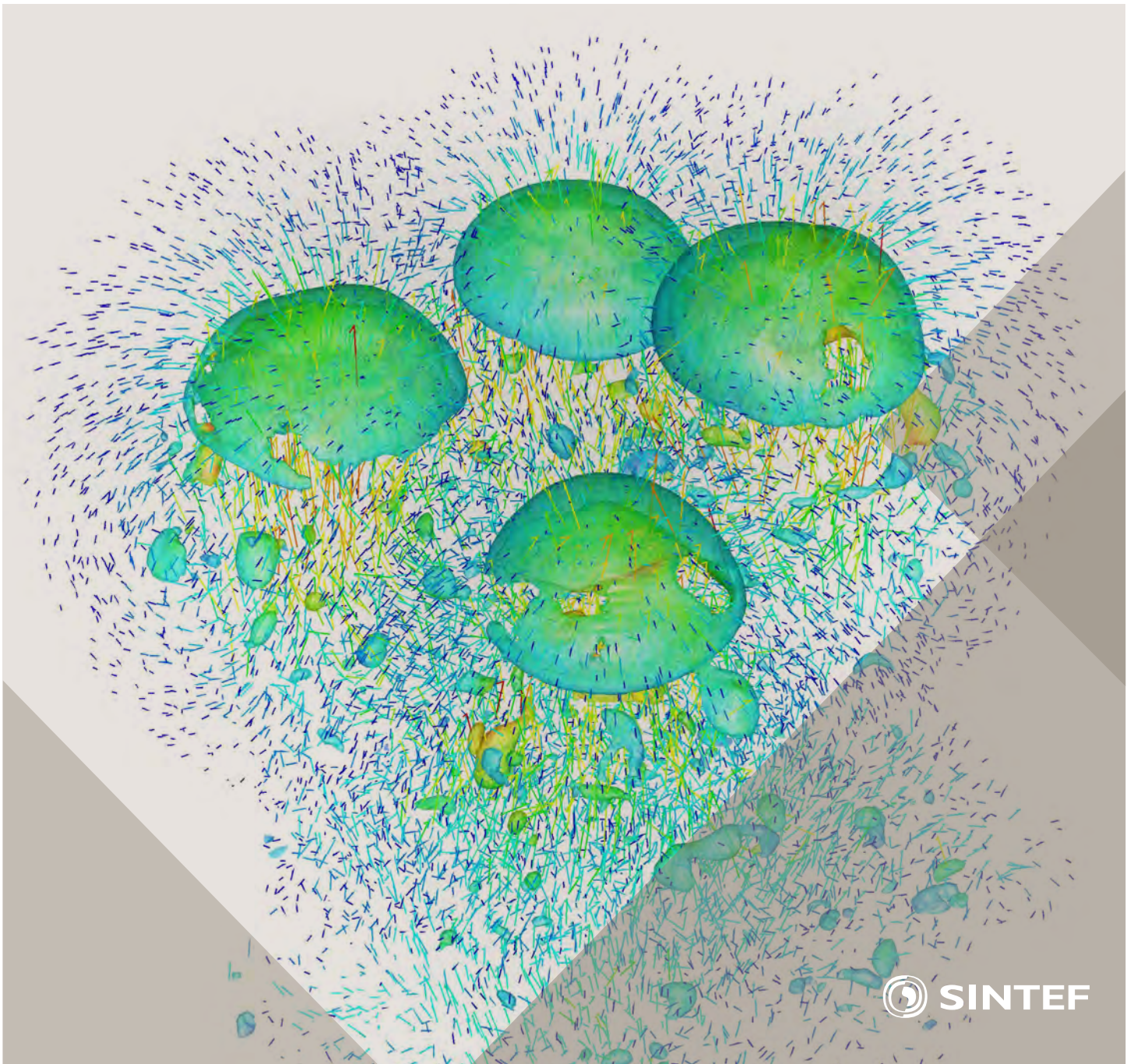
SINTEF

SINTEF Proceedings

Editors:
Jan Erik Olsen and Stein Tore Johansen

Progress in Applied CFD

Selected papers from 10th International Conference on Computational Fluid
Dynamics in the Oil & Gas, Metallurgical and Process Industries

SINTEF Academic Press

SINTEF Proceedings
SINTEF Proceedings is a serial publication for peer-reviewed conference proceedings
on a variety of scientific topics.
The processes of peer-reviewing of papers published in SINTEF Proceedings are
administered by the conference organizers and proceedings editors. Detailed procedures
will vary according to custom and practice in each scientific community.

PREFACE

This book contains selected papers from the 10th International Conference on Computational Fluid Dynamics in the Oil & Gas, Metallurgical and Process Industries. The conference was hosted by SINTEF in Trondheim in June 2014 and is also known as CFD2014 for short. The conference series was initiated by CSIRO and Phil Schwarz in 1997. So far the conference has been alternating between CSIRO in Melbourne and SINTEF in Trondheim. The conferences focus on the application of CFD in the oil and gas industries, metal production, mineral processing, power generation, chemicals and other process industries. The papers in the conference proceedings and this book demonstrate the current progress in applied CFD.

The conference papers undergo a review process involving two experts. Only papers accepted by the reviewers are presented in the conference proceedings. More than 100 papers were presented at the conference. Of these papers, 27 were chosen for this book and reviewed once more before being approved. These are well received papers fitting the scope of the book which has a slightly more focused scope than the conference. As many other good papers were presented at the conference, the interested reader is also encouraged to study the proceedings of the conference.

The organizing committee would like to thank everyone who has helped with paper review, those who promoted the conference and all authors who have submitted scientific contributions. We are also grateful for the support from the conference sponsors: FACE (the multiphase flow assurance centre), Total, ANSYS, CD-Adapco, Ascomp, Statoil and Elkem.

Stein Tore Johansen & Jan Erik Olsen

3

Organizing committee:

Conference chairman: Prof. Stein Tore Johansen
Conference coordinator: Dr. Jan Erik Olsen
Dr. Kristian Etienne Einarsrud
Dr. Shahriar Amini
Dr. Ernst Meese
Dr. Paal Skjetne
Dr. Martin Larsson
Dr. Peter Witt, CSIRO

Scientific committee:

J.A.M.Kuipers, TU Eindhoven
Olivier Simonin, IMFT/INP Toulouse
Akio Tomiyama, Kobe University
Sanjoy Banerjee, City College of New York
Phil Schwarz, CSIRO
Harald Laux, Osram
Josip Zoric, SINTEF
Jos Derksen, University of Aberdeen
Dieter Bothe, TU Darmstadt
Dmitry Eskin, Schlumberger
Djamel Lakehal, ASCOMP
Pär Jonsson, KTH
Ruben Shulkes, Statoil
Chris Thompson, Cranfield University
Jinghai Li, Chinese Academy of Science
Stefan Pirker, Johannes Kepler Univ.
Bernhard Müller, NTNU
Stein Tore Johansen, SINTEF
Markus Braun, ANSYS

CONTENTS

MODELLING THERMAL EFFECTS IN THE MOLTEN IRON BATH
OF THE HISMELT REDUCTION VESSEL

Peter J. WITT[1*], Yuqing FENG[1] and Mark P. DAVIS[2]

[1] CSIRO Mineral Resources Flagship, Melbourne 3169, AUSTRALIA

[2] HIsmelt Corporation Pty Ltd, Kwinana 6966, AUSTRALIA

* E-mail: peter.witt@csiro.au

ABSTRACT

Over a thirty year period the HIsmelt process has been developed as an alternative to the traditional blast furnace for the production of pig iron. This process involves the injection of fine iron ore and non-coking coal particles into a molten iron bath though a number of wall lances. These jets induce substantial mixing and splashing of molten droplets into the top space of the vessel due to the substantial volume of gas generated within the bath. Control of heat transfer, reactions and the complex multiphase fluid dynamics is critical to successful operation of the process. Since inception computational fluid dynamics has played an important role in scale-up and process optimisation (Davis *et al.* 2003, Davis and Dry, 2012).

A "Bath model" has been developed which focuses on the smelt-reduction processes occurring within the bath volume of the HIsmelt vessel (Stephens *et al.* 2011). As this model is a transient multi-component Eulerian-Eulerian model with Lagrangian particle tracking for the coal and ore particles, it requires a substantial computational effort. For this reason (and due to the large thermal inertia of the liquid bath) earlier versions of the model have been isothermal.

Particles enter the molten iron bath at close to ambient temperature. Heating of both the particles and gas stream by the bath will require a finite time and cause local cooling around the particle jet. To investigate this effect the bath model has been extended to include convective heat transfer between the bath, gas and particles, and radiation within the gas cavity.

This paper reports on the incorporation of thermal effects into the model and presents results showing their impact.

Keywords: CFD, Multiphase heat and mass transfer, Process metallurgy, HIsmelt process, Iron Making, Thermal Radiation.

NOMENCLATURE

Greek Symbols
α volume fraction.
ε energy dissipation rate, [$m^2 s^{-3}$].
λ thermal conductivity, [$W m^{-1} K^{-1}$].
ρ mass density, [$kg m^{-3}$].
ϕ_P particle diameter, [m].
τ stress tensor, [Pa].
μ viscosity, [$kg m^{-1} s^{-1}$].

Latin Symbols
A interfacial area [m^2].
Cp specific heat, [$J kg^{-1} K^{-1}$].
g gravitational acceleration, [$m s^{-2}$].
F_D, F_B particle drag and buoyancy force, [N].
h static enthalpy, [$J kg^{-1}$].
k turbulence kinetic energy, [$m^2 s^{-2}$].
m_p particle mass, [kg].
$M_{F,r}$ inter-phase drag force, [$N m^{-3}$].
p pressure, [Pa].
Q_C, Q_M, Q_R particle convective, mass transfer and radiation heat sources, [W].
Sc Schmidt number.
T temperature [K].
u_D, u_S drift and slip velocity, [$m s^{-1}$].
$\mathbf{u}$ velocity, [$m s^{-1}$].
$\mathbf{v}$ particle velocity, [$m s^{-1}$].
V_P particle volume [m^3].
$\mathbf{x}$ particle position, [m].
Y species mass fraction.

Sub/superscripts
g gas phase.
i chemical species index.
l liquid bath phase.
p particle phase.
r phase index.

INTRODUCTION

HIsmelt is a direct smelting technology for converting iron ore fines into pig iron. The process has been developed over a number of years and is slowly building into a serious challenge to the blast furnace. It offers the advantages of lower capital and operating costs, and greater raw material flexibility, whilst maintaining a high-quality metal product.

Development of the process has moved through a number of pilot plant designs to a commercial-scale facility of 0.8 Mt/a in Kwinana, Western Australia (2002-2008). All of these plant designs have been aided by the use of physical and CFD models. The plant is

currently being moved to Shandong in China to continue its development.

Scale up of any metallurgical process is problematic due to the increasing scales over which turbulent flow processes operate. Understanding the fluid dynamics involved and the associated heat and mass transfer has been critical to understanding and predicting the behaviour of the process and enabling the progression to larger smelting vessels.

CFD modelling of the HIsmelt Bath has been undertaken at the CSIRO for a number of years and has culminated in the development of the ANSYS/CFX thermal model presented in this paper.

MODEL DESCRIPTION

The domain for the CFD bath model includes the entire volume of the Smelt Reduction Vessel (SRV), illustrated in Figure 1, but the main focus is on ore reduction within the metal bath, coal devolatilisation and dissolution (into the metal), and the mass of liquid splashed into the gas space above the bath. Distinct gas, liquid and solid-particle phases are present in the computational domain and are critical to the smelting process and fluid dynamics behaviour. Each phase is comprised of a number of different components as summarised in Table 1 and Figure 2. There are large regions of continuous gas and similar volumes of continuous liquid; making the multi-fluid Eulerian-Eulerian approach the most appropriate way to model both the liquid bath and gas phases.
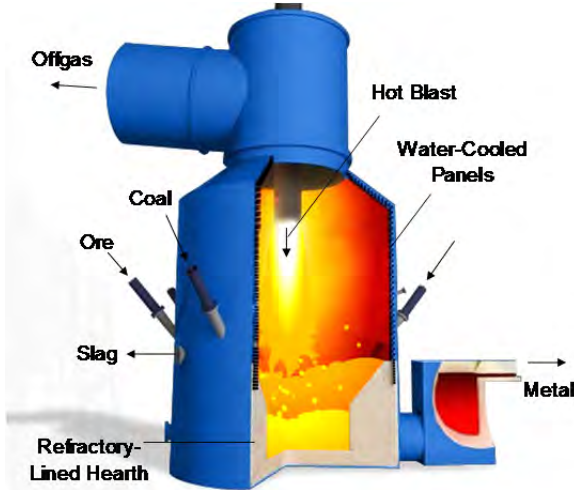

Figure 1: The HIsmelt Smelt Reduction Vessel.

The Eulerian-Eulerian model must simulate both the gas-continuous regions in which the liquid bath phase is assumed to be in dispersed form (splashes of droplets, fingers, sheets, etc in the upper regions of the SRV), as well as the liquid-continuous regions of the bath-proper in which the gas is assumed to be in the form of dispersed bubbles.

Within the gas phase a variable composition mixture is used to account for nitrogen (used as a carrier gas to inject the particles), carbon monoxide (evolved from ore reduction reactions) and hydrogen (evolved from coal devolatilisation). The liquid bath consists of two components, slag and metal. The slag is treated as a constant composition component, while the metal is

considered to be a variable composition mixture of iron and carbon. An Algebraic Slip Model (or mixture model in CFX terminology) is used to account for the relative motion of slag and metal (Fe/C melt), as first demonstrated in models of gas injection into a slag/metal bath by Schwarz and Taylor (1998).

Table 1: Phases and their compositions.

Phase	Type	Components
Gas	Eulerian	N_2, CO, H_2
Liquid Bath	Eulerian	Fe, Carbon, Slag
Ore particles	Lagrangian	Fe_2O_3, H_2O
Coal particles	Lagrangian	Coal fixed component, and Coal volatile component.

Iron ore and coal particles are modelled using the Lagrangian particle tracking approach. Iron ore particles are considered to be composed of hematite (Fe_2O_3) and moisture (H_2O). Coal particles are a variable composition mixture of fixed carbon and volatile carbon.
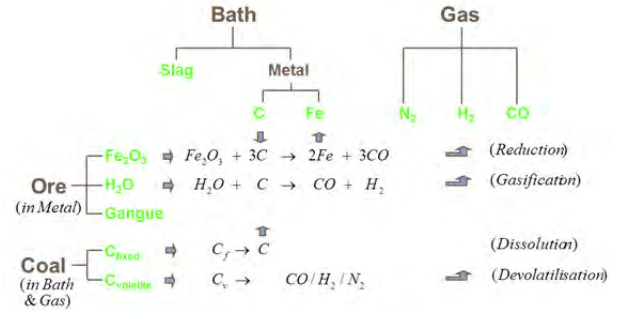
Figure 2: Schematic of the phase and component descriptions and associated reactions.

The reduction process is described by a series of idealised chemical reactions representing coal dissolution (into the molten iron):

$$C_{coal(sol)} \Rightarrow C_{metal} \tag{1}$$

coal devolatilisation (evolution of gaseous volatiles):

$$C_{vol(sol)} \Rightarrow CO + N_2 + H_2 \tag{2}$$

iron ore reduction (by dissolved carbon in the bath to form molten iron and carbon monoxide gas):

$$Fe_2O_{3\,ore} + 3C_{metal} \Rightarrow 2Fe_{metal} + 3CO \tag{3}$$

and gasification (water vapour in the ore particles reacts with dissolved carbon in the metal, generating hydrogen and carbon monoxide gas):

$$C_{metal} + H_2O_{ore} \Rightarrow H_2 + CO \tag{4}$$

Model Equations

For each Eulerian phase (gas and liquid-bath) continuity and momentum equations are solved to calculate the phase velocity, volume fraction and turbulence level. These transport equations can be written as:

Continuity equation with mass transfer

$$\frac{\partial}{\partial t}(\alpha_r \rho_r) + \nabla \cdot (\alpha_r \rho_r \mathbf{u}_r) = S_r \tag{5}$$

Here, the phases r are liquid bath phase ($r=l$) and gas phase ($r=g$). The term S_r is the net mass transfer to phase r from other interacting phases due to various reactions (described in detail in sections below).

Momentum equation

$$\frac{\partial}{\partial t}\left(\rho_r \alpha_r \mathbf{u}_r\right) + \nabla \cdot \left(\rho_r \alpha_r \mathbf{u}_r \mathbf{u}_r\right) \tag{6}$$
$$= -\nabla \cdot \left(\alpha_r \tau_{ij,r}\right) - \alpha_r \nabla P + \alpha_r \rho_r g + M_{F,r} + MS_r'$$

$$\sum \alpha_r = 1 \tag{7}$$

The terms on the right hand side of the momentum equation, (equation 6), represent respectively the stress, pressure gradient, gravity, momentum exchange between the phases due to interfacial forces (only the drag force is considered here) and the net momentum transfer to phase r by other phases due to net mass transfer (MS_r'). Pressure is shared by both the phases. The stress term for phase r is described as follows:

$$\tau_{ij,r} = -\mu_{eff,r}\left(\nabla \mathbf{u}_r + \left(\nabla \mathbf{u}_r\right)^T - \frac{2}{3}I(\nabla \cdot \mathbf{u}_r)\right) \tag{8}$$

The effective viscosity for each phase, $\mu_{eff,r}$ is composed of two contributions: the molecular viscosity and the turbulent viscosity. The turbulent eddy viscosity is formulated using the k-ε turbulence model and turbulence is considered homogeneous across both phases (k and ε values are the same for each phase):

$$\mu_{T,r} = \rho_r C_\mu \frac{k^2}{\varepsilon} \tag{9}$$

The turbulence kinetic energy (k) and its energy dissipation rate (ε) are calculated from their governing transport equations (equations 10 and 11 respectively). The term τ_m in these equations (as computed by equation 14) takes into account the phasic turbulent viscosity (equation 9) and the molecular viscosity of each phase.

$$\frac{\partial \rho_m k}{\partial t} + \nabla \cdot \left(\rho_m \mathbf{u}_m k\right) = -\nabla \cdot (\Gamma_m \nabla k) + (G_m - \rho_m \varepsilon) \tag{10}$$

$$\frac{\partial \rho_m \varepsilon}{\partial t} + \nabla \cdot \left(\rho_m \mathbf{u}_m \varepsilon\right) = -\nabla \cdot (\Gamma_m \nabla \varepsilon) + \frac{\varepsilon}{k}(C_{\varepsilon 1} G_m - C_{\varepsilon 2} \rho_m \varepsilon) \tag{11}$$

where

$$\rho_m = \rho_l \alpha_l + \rho_g \alpha_g \tag{12}$$

$$u_m = u_l \alpha_l + u_g \alpha_g \tag{13}$$

$$\tau_m = \tau_l \alpha_l + \tau_g \alpha_g \tag{14}$$

The model constants used are the standard values, viz. C_μ =0.09; σ_k=1.00; σ_ε=1.00; $C_{\varepsilon 1}$=1.44, $C_{\varepsilon 2}$=1.92. The term G in above equation is the production of turbulence kinetic energy and described by:

$$G = \tau_m : \nabla u_m \tag{15}$$

Thermal Energy Transport

Conservation of thermal energy in the gas and liquid phases is calculated by solving for the phase static enthalpy, h_r :

$$\frac{\partial}{\partial t}(\alpha_r \rho_r h_r) + \nabla \cdot (\alpha_r \rho_r \mathbf{u}_r h_r) =$$
$$\nabla \cdot (\alpha_r (\lambda_r + \lambda_r^t)\nabla T_r) +$$
$$S_{h,r} + SH_{p,r} + SH_{m,r} + S_{rad,r} \tag{16}$$

where $\lambda_r + \lambda_r^t$ are the molecular and turbulent thermal conductivities, T_r is the temperature for phase r and source terms $S_{h,r}$, $SH_{p,r}$, $SH_{m,r}$, $S_{rad,r}$ are for energy transfer between phases, to and from particles, particle mass transfers and thermal radiation. Static enthalpy and temperature are related through the phase specific heat, Cp_r, by:

$$h_r = Cp_r T_r \tag{17}$$

Thermal radiation transport is calculated using the Discrete Transfer model of Shah (1979) and provides source terms for the phase-enthalpy and particle transport equations. A high value for the absorption coefficient is set for the liquid phase. This effectively limits radiation transport to within the gas only volumes and to/from the liquid surfaces.

Species Transport

Mass fractions of individual components (CO, N_2) in the multi-component gas phase are computed by solving each component's transport equation (equation 18) with relevant source/sink terms, while the mass fraction of H_2 in the gas phase is determined using constraint equation 19.

$$\frac{\partial \alpha_g \rho_g Y_{gi}}{\partial t} + \nabla \cdot \left(\alpha_g \rho_g u_g Y_{gi}\right) = \nabla \cdot \Gamma_{gi} \alpha_g \nabla Y_{gi} + S_{gi} \tag{18}$$

$$\sum Y_{gi} = 1 \tag{19}$$

where Y is the mass fraction of species i in the r phase. Similarly, the mass fraction of individual components (Fe, C and slag) in the multi-component liquid phase is obtained by applying the algebraic slip model (ASM, equation 20 and 21). This is done in order to enable the separation of slag from metal. The slag is considered to be continuous in the liquid bath and its fraction is computed using constraint equation 22. The ASM enables computation of a slip velocity between metal (Fe/C) and slag, and the drift velocity of Fe/C. The drift velocity of a component is taken relative to the mixture (i.e. the liquid bath) velocity, whereas the slip velocity of a component is taken relative to the velocity of continuous medium in the mixture (i.e. slag velocity in this case).

$$\frac{\partial \alpha_l \rho_l Y_{li}}{\partial t} + \nabla \cdot \left(\alpha_l \rho_l (u_l + u_{Di})Y_{li}\right) = \nabla \cdot (\Gamma_{li} + \frac{\mu_t}{Sc_t})\alpha_l \nabla Y_{li} + S_{li} \tag{20}$$

where, u_{Di} is the drift velocity of species i, and is related to the slip velocity u_{Si} by equation 21.

$$u_{Di} = u_{Si} - \sum_i u_{Si} Y_{li} \tag{21}$$

$$\sum Y_{li} = 1 \tag{22}$$

Lagrangian particle tracking of ore and coal

The velocities, trajectories and temperatures of representative ore and coal particles are computed using the Lagrangian tracking approach, originally developed by Crowe *et al.* (1977), which involves solving the momentum equations based on Newton's second law (equations 23 to 25) and a particle temperature equation 26. Ore and coal particles are treated as separate phases. The interaction between the carrier fluid and particles has been treated using two-way coupling. The carrier fluid for particles can be the Eulerian gas phase or the Eulerian liquid bath phase, the appropriate phase being decided based on a critical volume fraction of these phases at the location of the particle. Particle drag and heat transfer switches from gas to liquid at this critical voidage. Equations 23 and 24 compute the particle displacement using forward Euler integration of particle velocity over the time-step. In forward integration, the particle velocity is calculated at the start of the time step and is assumed to prevail over the entire time step. At the end of the time step, the new particle velocity is computed using the particle momentum equation 25. Momentum is transferred between fluid and particles only through the inter-phase forces. In general these forces would be drag force, added mass force, pressure force, buoyancy force and Basset force. In this work, only drag and buoyancy has been considered, as they are the dominant forces.

$$\frac{dx_i}{dt} = v_i \tag{23}$$

$$x_i^n = x_i^0 + v_i^0 \partial t \tag{24}$$

$$\frac{d(m_p v_i)}{dt} = F_D + F_B \tag{25}$$

$$\frac{d(m_p C_p T_p)}{dt} = Q_C + Q_M + Q_R \tag{26}$$

The effect of turbulent dispersion on particle motion has been included for the gas phase but not the liquid phase as particle motion in the latter is dominated by the drag force. The mass, momentum and energy sources transferred by the particles to the phase in contact (gas or bath) are determined by the reactions occurring (ore reduction, coal devolatilisation and coal dissolution). Similarly, energy sources between particle and the phase in contact are computed using the Ranz and Marshall (1952) model for convective heat transfer, Q_C, and the Discrete Transfer model calculates the radiation sources, Q_R. These particle sources are applied in the control volume in which the particle is located during the time step. These sources are then applied each time the fluid coefficients are calculated.

Interfacial mass, momentum and energy exchange

The following phase-pairs interact during the simulations and exchange mass, momentum and energy:

Bath-Gas, Ore-Gas, Ore-Bath, Coal-Gas and Coal-Bath

The drag force, $M_{F,r}$, between the liquid bath and gas is computed using a user-defined drag function derived from experimental models (Schwarz, 1996). Convective heat transfer between the gas and bath, $S_{h,r}$, is calculated as:

$$S_{h,g} = -S_{h,l} = \frac{(\alpha_l \lambda_l + \alpha_g \lambda_g) \text{Nu}}{\phi_B} \frac{(\alpha_l + \alpha_g)}{\phi_B}\left(T_l - T_g\right) \tag{27}$$

with the Nusselt number, Nu, calculated from the correlation of Tomiyama (1998):

$$\text{Nu} = 2.0 + 0.15 \text{Re}^{0.8} \text{Pr}_l^{0.5} \tag{28}$$

where Re is the bubble Reynolds number and Pr_l is the bath Prandtl number.

For ore–gas phase and ore-liquid phase interaction, the drag force coefficient is computed using the Schiller and Naumann (1935) drag model.

For a coal particle that undergoes devolatilisation or dissolution, coal particle porosity is computed and used in a modified Schiller-Naumann model in which the particle diameter remains constant (i.e. there is no swelling of the coal particle).

Convective heat transfer, Q_C, between a coal or ore particle and the fluid phase is calculated from:

$$Q_C = \pi \phi_P \lambda_r \text{Nu}_p (T_r - T_P) \tag{29}$$

with the Nusselt Number, Nu_p, given by the Ranz and Marshall (1952) correlation:

$$\text{Nu}_p = 2 + 0.6 \text{Re}_p^{0.5} \text{Pr}_r^{0.3} \tag{30}$$

where Re_p is the particle Reynolds number and Pr_r the Prandtl number for the fluid phase, r, the particle is in contact with. From Q_C the source terms, $SH_{p,r}$, for equation (16) is determined by multiplying by the number of particles in the fluid control volume.

Mass transfer that arises due to particle reactions produces source terms in the continuity equation, S_r, (equation 5) momentum equation, MS_r (equation 6) and the energy equation, $SH_{m,r}$ (equation 16). The mass transferred is dependent upon the rate of reaction of each reaction. These reactions are now discussed in more detail.

Coal devolatilisation reaction

$$\begin{aligned} \text{Coal}_{(s)} \rightarrow \text{Volatiles}_{(g)} \quad &+ \quad \text{Char}_{(s)} \\ \{CH_4, H_2O, \text{etc}\} \quad &\quad \{C + \text{ash}\} \end{aligned} \tag{31}$$
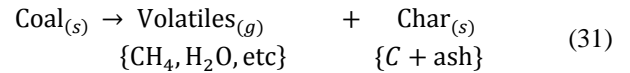
This reaction is simplified to:

$$\begin{aligned} \text{Coal}_{(s)} &\rightarrow aCH_4 + bC_{(s)} \\ &\{\text{cracking}\} \\ &\rightarrow \quad xC_{(s)}\{\text{soot}\} + yH_{2(g)} + zC_{(s)}\{\text{char}\} \end{aligned} \tag{32}$$
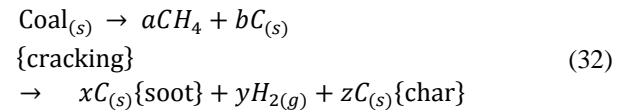
Although soot will behave differently from char, it is assumed that within the bath the soot will react with oxygen to form CO. This has been assumed to also occur within the gas phase, although in reality some soot will escape with the gas into the topspace.

$$\text{Coal}_{(s)} \Rightarrow aC_{(s)} + bCO + cH_2 + dN_2 \tag{33}$$
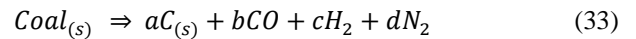
The main aim of including devolatilisation in the bath model is to allow for the generation of large volumes of volatiles gas within the bath and to simulate the spatial distribution of this generation. Data from the literature have been used to give a simple representation of the way coal particles devolatilise. A simplified linear fit to

the Oeters and Orsten (1989) results was implemented in previous CFD models (Schwarz, 1994, Stephens *et al.* 2011).

With the inclusion of thermal effects into the model, combined with the endothermic nature of coal devolatilisation and the low heat capacity of the gas, it is possible that cooling of the particles could occur as volatiles are released. If the reaction is too fast then the particle temperature can drop to unphysical values. The model of Oeters assumes that the particle is injected directly into the liquid bath and that it heats up to close to the bath temperature before evolving volatiles. Once volatiles are released they form a gas bubble in which the particle is located. Hence the heat transfer and mass transfer to and from the particle are through gas in the bubble surrounding the particle. This would suggest that the reaction rate from Stephens *et al.* (2011) is the maximum rate and would also apply in a turbulent gas stream that was at the bath temperature.

However at lower temperatures the reaction rate would reduce. Assuming that the model from Stephens *et al.* (2011) gives the maximum rate then a reduction factor could be applied to that rate depending on particle temperature. Using an Arrhenius model and arbitrarily assuming that no reaction occurs below 500°C and the maximum rate is achieved at 1200°C, the reduction function is:

$$f(T_p) = 60e^{\frac{-6000}{T_p}} \qquad (34)$$

where T_p is the particle temperature [K]. This function is plotted in Figure 3.
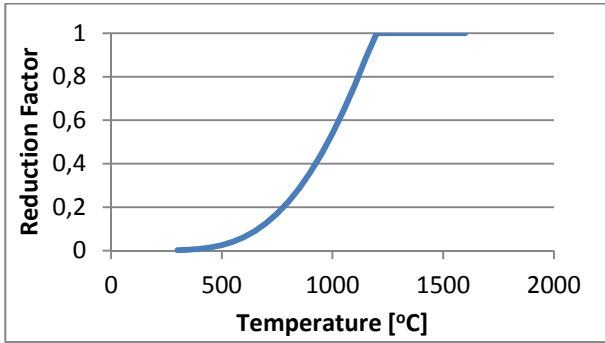

Figure 3: Reduction function, $f(T_p)$.

The overall rate of the devolatilisation reaction for each track is then given by:

$$Rate = \frac{dm}{dt} = 60e^{\frac{-6000}{T_p}} \frac{C_{coalvolatile} V_p \, \rho_p}{0.35 \times 1.05(\emptyset_p)^{1.5}} \qquad (35)$$

where V_p is the initial volume of the particle in the track.

Coal Dissolution

Coal dissolution (equation 1) is only allowed to occur between coal particles and metal. Furthermore it is assumed that it only occurs after devolatilisation is complete. In reality, some of the coal will not contact metal, but will rather react in the slag. The metal volume fraction is used to weight the reaction rate, R_{coal}, which is given by:

$$\frac{dR_{coal}}{dt} = A_{p,coal} \rho_l \chi (C_{carbon,sat} - C_{carbon}) Y_{metal} \qquad (36)$$

where $A_{p.coal}$ is the coal particle interfacial area, ρ_l is the liquid density, χ is the mass transfer coefficient for liquid side transport, $C_{carbon,sat}$ is the saturation carbon concentration in the bath, C_{carbon} is the carbon concentration in the vicinity of the particle and Y_{metal} is the metal mass fraction in the vicinity of the particle. The particles shrink as they dissolve, so the interfacial area is:

$$A_{p,coal} = \pi \emptyset_{p,coal}^2 \qquad (37)$$

Ore Dissolution

Equation 3 describes the ore reduction and dissolution process. Here, we simplify by assuming that all the iron (Fe) produced reports to the metal phase. In reality, some ore will melt as FeOx in slag. The equation for the mass reaction rate, R_{ore} is:

$$\frac{dR_{ore}}{dt} = A_{p,ore} \rho_l \chi C_{carbon} Y_{metal} \frac{196}{36} \qquad (38)$$

where $A_{P.ore}$ is the ore particle interfacial area. The particles shrink as they dissolve, so the interfacial area is again given by:

$$A_{p,ore} = \pi \emptyset_{p,ore}^2 \qquad (39)$$

The stoichiometric mass coefficients in equation 3 are:

$$MC_{Fe_2O_3} = \frac{160}{196}; MC_C = \frac{36}{196}; MC_{Fe} = \frac{112}{196}; MC_{CO} = \frac{84}{196}.$$

The mass transfer coefficient, χ, is estimated based on reported reaction rates measured for ore reduction by Nagasaka and Banya (1992). Table 2 summarizes the discussions above.

Table 2: Reaction physics summary.

Material	Reaction	Location	Depends on
Coal	Devolatilisation	Bath and Gas	Temperature and particle diameter. Particle diameter remains constant.
	Dissolution	Bath (Metal)	Carbon concentration in the Bath. Liquid side mass transfer control. Particle diameter reduces.
Ore	Reduction	Metal	Carbon concentration in the bath. Liquid side mass transfer control. Particle diameter reduces.

Numerical Model

The commercial code ANSYS/CFX (ANSYS, 2010) is used to solve the equations and physical models described above. ANSYS/CFX 13 uses a finite volume method to iteratively solve the above equations on an unstructured grid. Coupling between pressure, velocity and phases is handled implicitly by the CFX coupled volume fraction solver. The second order accurate "Compressive Scheme" was used to discretise advection terms in the equations to improve solution accuracy.

A second order backward Euler implicit time integration scheme was used to advance transient terms in the

equations. An initial time step of 0.0005 seconds was used to advance the solution in time for the first few time steps. Due to the highly transient nature of the flow with splashing and gas evolution an adaptive time stepping strategy was used to minimise computational time and ensure convergence at each time step. After the initial start up transient the typical time step was 0.001 seconds with on average 6 coefficient loops required at each time step to reduce the residuals below 2×10^{-4} RMS and to achieve the conservation target.

Density for the gas phase is calculated based on the perfect gas law and is a function of composition, pressure and temperature. The liquid bath was assumed incompressible. At wall boundaries scalable turbulent wall functions were used to capture near wall effects.

The simulations were run on quad core dual CPU, 3.6GHz Intel Westmere processors installed in CSIRO's CFD cluster. The model was run for 10 seconds of simulated time on 16 parallel partitions. Total wall time for the simulation was approximately 8 days. Further details of the numerical approach and implementation are described in ANSYS (2010).

GEOMETRY, BOUNDARY AND INITIAL CONDITIONS

The model described above was applied to the HIsmelt Research and Development Facility (HRDF) pilot plant reactor. Internal diameter of the reactor is 2.7 m in the hearth and 5.1 m in the top space with a height of roughly 6 m. To reduce the model size and run time a vertical symmetry plane is used through the centre of the lances. Model geometry is shown in Figure 4. Coal and ore particles are injected through the base of the lances with a nitrogen carrier gas at a temperature of 30°C and velocity of 80.4 ms^{-1}. The particle size distribution is accounted for using a Rosin-Rammler distribution with the coal mean diameter being 294 µm and an ore mean diameter of 1112 µm. Particles are uniformly injected from the lance exits at a rate proportional to their mass flow rate. Gas can leave the domain through a pressure boundary at the offgas outlet.
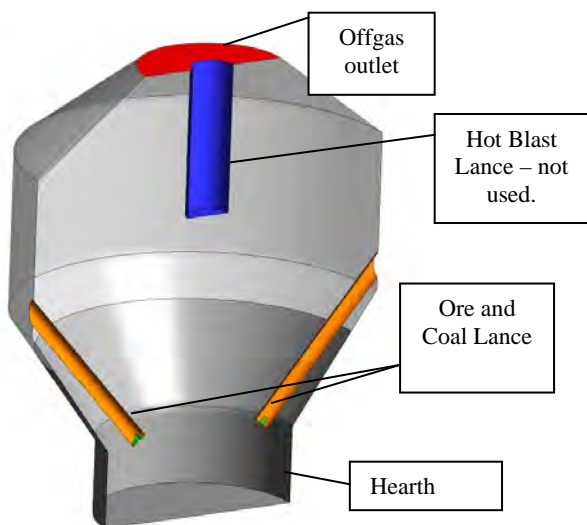
Figure 4:   HIsmelt SRV geometry.

The mesh for the domain consists of over 45,000 nodes and 255,000 tetrahedral elements. An indication of the mesh resolution is shown in Figure 5 for the symmetry

plane and shows the refinement used to capture the steep gradients at the lance exits.

Initial conditions for the simulation set the gas and bath temperatures at 1437°C, the metal height is 530 mm and slag depth above the metal is 1189 mm. The bath is assumed quiescent with no gas bubbles or cavities and contains no particles.

RESULTS

The model described above was run for 10 seconds of real time and the predicted gas distributions at four time instants are plotted in Figure 6. Gas injection and more significantly gas generation from the particles induces complex flow behaviour such as splashing and formation of a fountain in the top space of the vessel. Such behaviour is consistent with previous iso-thermal model results such as Stephens *et al.* (2011).
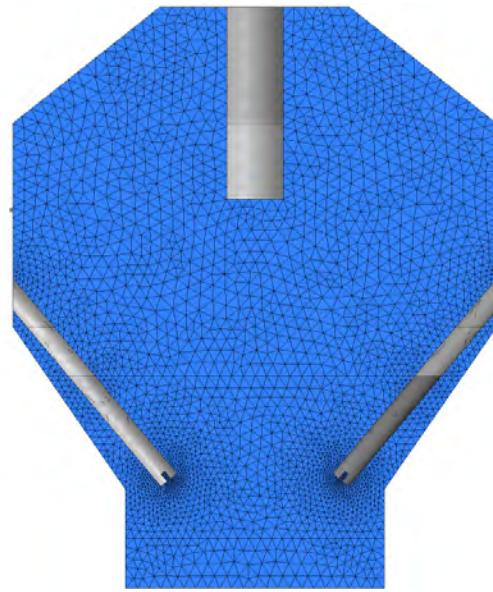

Figure 5:   Symmetry plane mesh.

In this work we have extended the previous work by including heat transfer, and have predicted gas temperature distributions that are at the same time plotted in Figure 7. Black contour lines for a gas volume fraction of 0.8 are superimposed over the temperature plots. Particles and carrier gas enter the vessel at 30 °C and gas is heated rapidly to the bath temperature. However cavities with gas temperatures below 500 °C occur directly above the lances and a cool jet below 100 °C is predicted for a couple of lance diameters downstream of the lance tips. As shown by the liquid bath temperature plots in Figure 8, bath temperature remains nearly constant with only drops entrained into the gas cavities near the lance and in the top space experiencing some cooling.

Temperature of typical coal particles is plotted in Figure 9 up to a time of 9.14 seconds. Figure 9a shows how coal particles larger than 200 µm in the gas phase penetrate a significant distance into the bath and generally do not experience a rapid rise in temperature. Smaller coal particles, in Figure 9b, only partially penetrate the bath; with many being entrained by gas plumes into the top space where they undergoing heating. Many particles contact the bath and in the model are reborn into the liquid phase.

| t= 0.046 [s] | t =0.47 [s] | t = 2.4 [s] | t = 9.14 [s] |
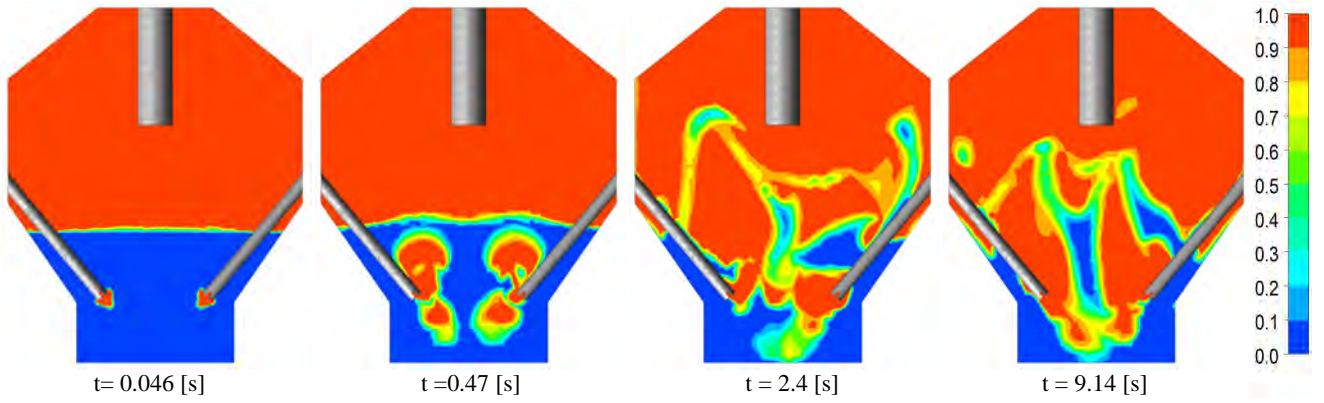
Figure 6: **Gas volume fraction at various times.**

| t = 0.046 [s] | t =0.47 [s] | t = 2.4 [s] | t = 9.14 [s] |
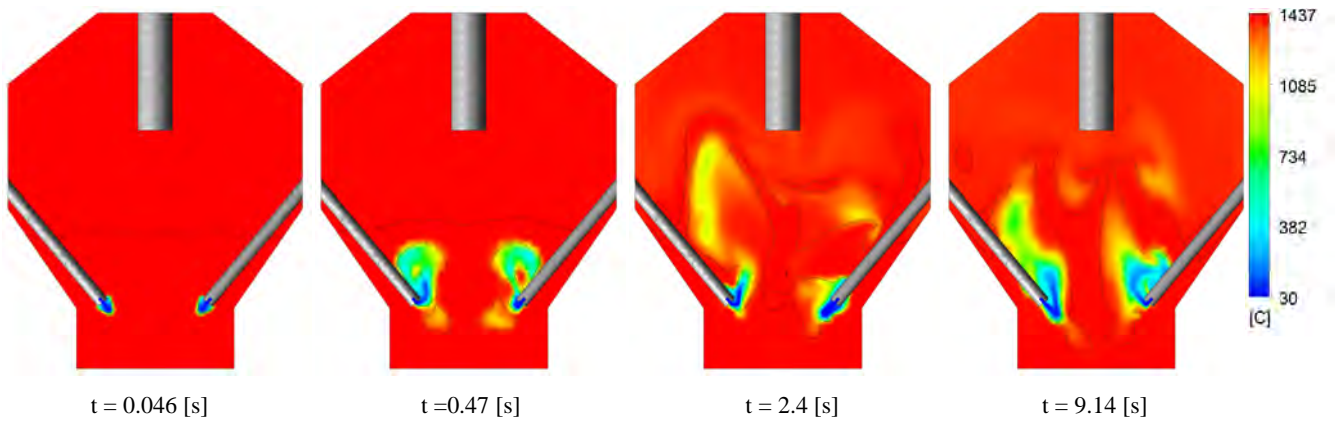
Figure 7: **Gas temperature at various times.**

| t = 0.046 [s] | t =0.47 [s] | t = 2.4 [s] | t = 9.14 [s] |

Figure 8: **Bath temperature at various times.**

| (a) >200 µm in gas | (b) ≤200 µm in gas | (c) >200 µm in bath | (d) ≤200 µm in bath |
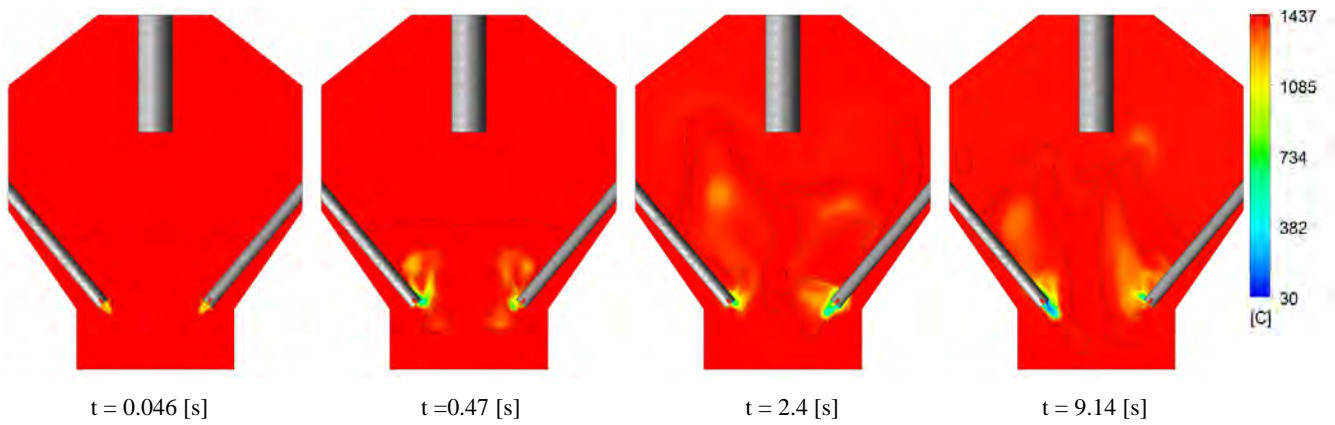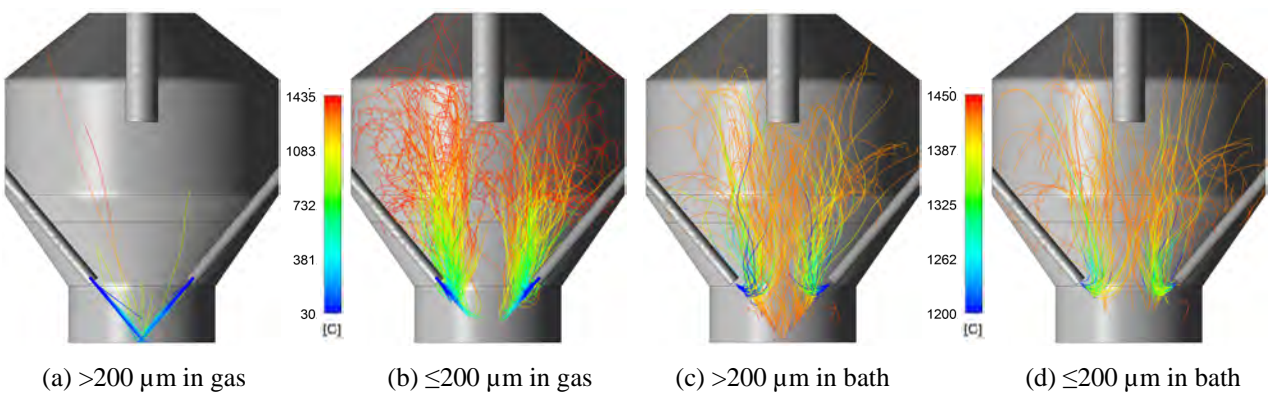
Figure 9: **Coal particle temperatures up to a time of 9.14 [s].**

Temperatures for coal particles in the liquid are shown in Figure 9(c) and (d). Note the different temperature scales used for particles in the gas and liquid phases. It is also apparent that once particles contact the liquid bath they undergo rapid heating; this is for both small and large particles.

Temperatures of the larger diameter ore particles are plotted in Figure 10. With a mean diameter of 1112 µm ore particles do not experience a large temperature rise until they enter the liquid bath. They also penetrate into the liquid bath without being entrained into the top space with the gas.
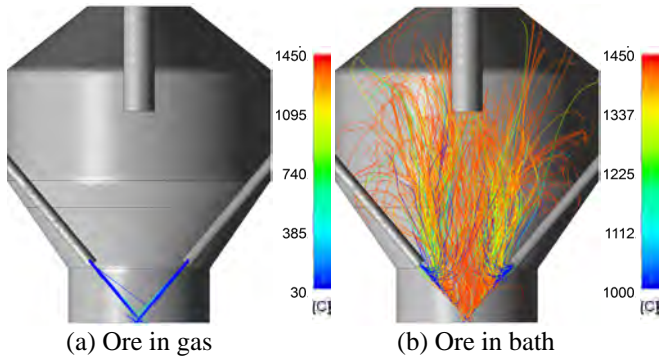

(a) Ore in gas   (b) Ore in bath
Figure 10: Ore particle temperatures to a time of 9.14 [s].

Heating of the coal particles results in devolatilisation and the release of volatiles; the change in coal volatile mass fraction is plotted in Figure 11 for the same particle groups shown in Figure 9. Large particles in the gas phase undergo little volatile release due to the slow heating rate, see Figure 11a; but once they enter the bath, as shown in

Figure 11c, they rapidly evolve their volatiles. Smaller particles in the gas phase undergo devolatilisation more rapidly than the larger particles in the gas, as shown in Figure 11b, but not as fast as large particles in the bath phase. When small particles contact and enter the bath they undergo rapid devolatilisation, Figure 11d, with most of the volatiles being released near the lance tip.

Rapid devolatilisation of the coal produces large gas source terms that are primarily carbon monoxide and hydrogen. Plots of the CO and H_2 mass fractions in the gas phase are shown in Figures 12 and 13. In Figure 6 at 0.47 seconds a gas cavity has formed below the lance with a region of liquid between the cavity and lance tip. An analysis of results at 25 ms intervals shows the cavity is formed by coal particles penetrating the liquid bath and devolatilising within the liquid. This can also be seen by the high CO and H_2 concentrations in Figures 12 and 13 at 0.47 seconds.

Model Validation

Given the nature of the HIsmelt process (i.e. high temperature, molten splash, heterogeneous reactions) model validation will always be problematic. In addition, thermal transients in the process (such as bath temperature) occur over longer time scales than can be currently simulated (due to the complexity of the model). Model validation has relied on gaining confidence in various aspects of the two-phase model during development by comparing with small scale water, iron and tin models (e.g. Schwarz 1996). Plant data is also used where possible to verify model predictions. For
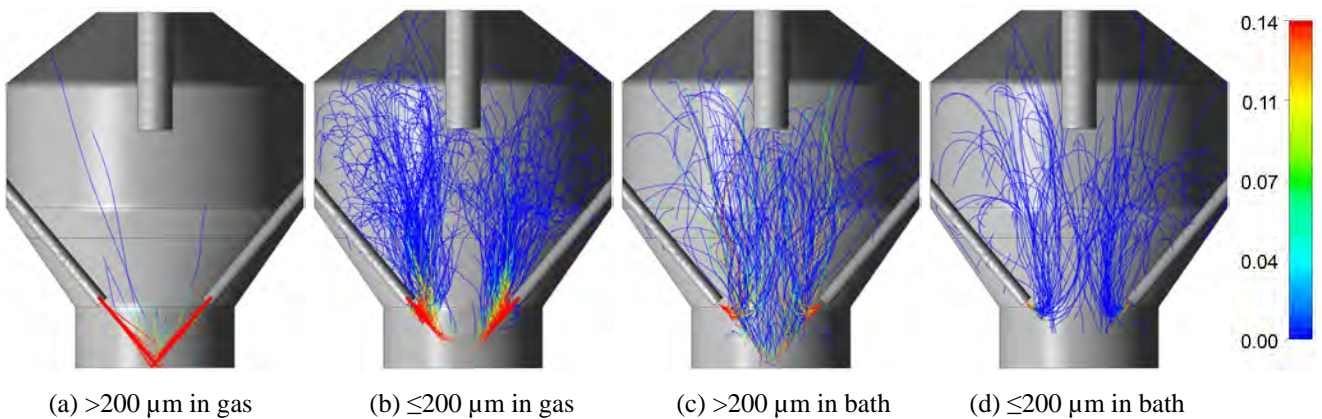
(a) >200 µm in gas   (b) ≤200 µm in gas   (c) >200 µm in bath   (d) ≤200 µm in bath
Figure 11:   Coal particle volatile mass fraction to a time of 9.14 [s].
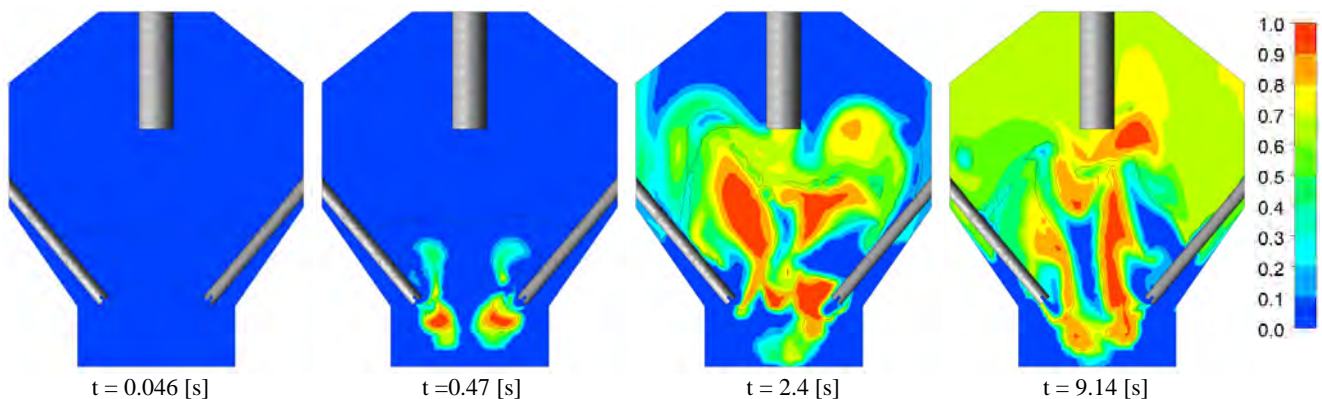
t = 0.046 [s]   t =0.47 [s]   t = 2.4 [s]   t = 9.14 [s]
Figure 12:   Carbon monoxide mass fraction at various times.

| t = 0.046 [s] | t =0.47 [s] | t = 2.4 [s] | t = 9.14 [s] |
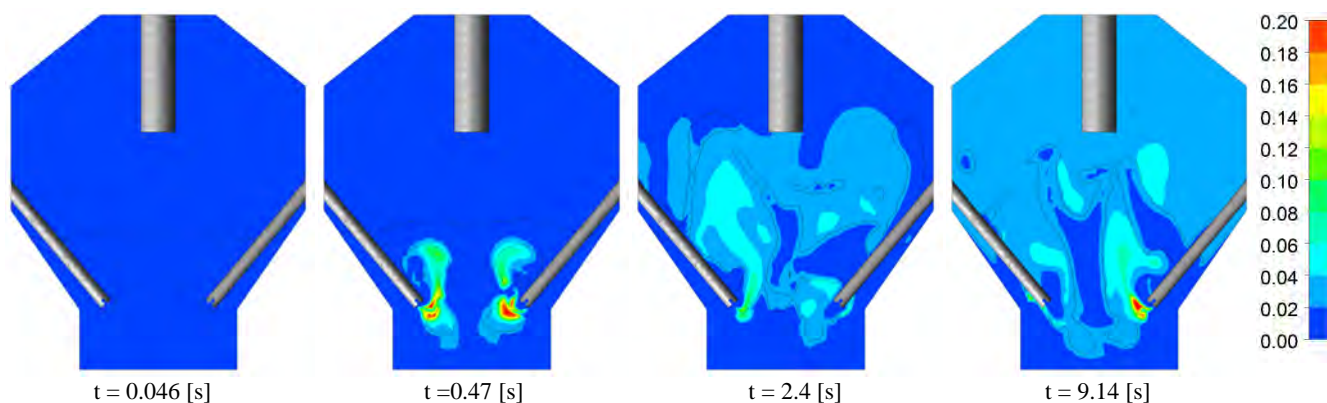
**Figure 13: Hydrogen mass fraction at various times.**

example, Figures 9(a) and 10(a) indicate that feed particles penetrate to the bottom of the bath. This is corroborated by wear of the refractory bricks at the centre of the hearth floor found during operation of the HRDF plant.

CONCLUSION

Multiphase fluid dynamics and heat transfer within the HIsmelt vessel are critical to plant operation and performance. Understanding these processes is critical to scale-up and further development of the HIsmelt process. A previously developed isothermal model of the bath has been extended to include heat transfer processes for both convection and radiation so as to allow the prediction of temperature distributions and particle heating rates.

Model results show that bath temperature is relatively constant and that cooler gas cavities exist near and above the lance tips. Coal particles undergo rapid heating once they enter the liquid bath, which causes rapid devolatilisation leading to the formation of gas cavities below the liquid surface. Particles in the gas smaller than 200 µm in diameter were found to increase in temperature and undergo devolatilisation. Larger coal particles tended to only devolatilise once they contracted the liquid bath. This work indicates that, while adding to computational cost, inclusion of thermal effects can be important for particle heating rates and gas generation within the bath and subsequent bath dynamics.

ACKNOWLEDGMENTS

REFERENCES

ANSYS Workbench / Fluent 13.0, ANSYS Inc., USA. 2010.

CROWE, C. T., SHARMA, M. P. and STOCK, D. E., (1977), "The Particle-Source-in-Cell (PSI-CELL) Model for Gas-Droplet Flows", *J. Fluids Eng.*, **99**, 325-332.

DAVIS, M., and DRY, R., (2012), "CFD modelling in the development and scale-up of the HIsmelt process", 9th *Int. Conference on CFD in the Mineral and Process Industries,* CSIRO, Melbourne, Australia, 10-12 Dec.

DAVIS, M., DRY, R., and SCHWARZ, M.P., (2003), "Flow Simulation of the HIsmelt Process", *3rd Int. Conference on CFD in the Mineral and Process Industries,* CSIRO, Melbourne, Australia, 10-12 Dec.

NAGASAKA, T. and BANYA, S., (1992), "Rate of Reduction of Liquid Iron Oxide", *Tetsu-to-Hagane*, **78**, 1753-1767.

OETERS F., and ORSTEN S., (1989), "Degassing of coal particles injected into iron melts", *Steel Research*, **60**, 145-150.

RANZ, W.E. and MARSHALL, W.R., (1952), "Evaporation from drops", *Chem. Eng. Prog.* **48**, 141-146.

SCHILLER, L. and NAUMANN, Z., (1935), "A Drag Correlation", *Z. Ver. Deutsch. Ing.*, **77**, 318.

SCHWARZ, M.P., (1994), "The role of Computational Fluid Dynamics in process modeling", *Proc. of 6th AusIMM Extractive Metallurgy Conference*, pages 31-36, Aus.IMM, 1994.

SCHWARZ, M.P., (1996), "Simulation of Gas Injection into Liquid Melts", *Applied Mathematical Modelling*, **20**, 1996, 41-51.

SCHWARZ, M.P. and TAYLOR, I. F., (1998), "CFD and Physical Modelling of Slag-Metal Contacting in a Smelter", *4th World Conference on Applied Fluid Mechanics*, Freiburg, Germany: WUA-CFD, 4:1-4:15.

SHAH, N.G., (1979), "A New Method of Computation of Radiant Heat Transfer in Combustion Chambers", *PhD thesis*, (Imperial College of Science and Technology, London).

STEPHENS, D., TABIB, M., DAVIS, M., and SCHWARZ, M.P., (2011), "CFD Simulation of Bath Dynamics in the HIsmelt Smelt Reduction Vessel for Iron Production", *8th Int. Conference on CFD in Oil & Gas, Metallurgical and Process Industries,* SINTEF/NTNU, Trondheim, Norway, 21-23 June.

TOMIYAMA, A., (1998), "Struggle with computational bubble dynamics". Third International Conference on Multiphase Flow, Lyon, France. June 8-12.